Computerized Medical Imaging and Graphics 36 (2012) 580–588

Contents lists available at SciVerse ScienceDirect

Computerized Medical Imaging and Graphics

journal homepage: www.elsevier.com/locate/compmedimag

Automated TIMI frame counting using 3-d modeling

G.A. ten Brinke[a,*], C.H. Slump[a,1], M.G. Stoel[b,2]

[a] Signals and Systems, University Twente Enschede, The Netherlands
[b] Thorax Center, Medisch Spectrum Twente Enschede, The Netherlands

ARTICLE INFO

Article history:
Received 19 December 2011
Received in revised form 15 June 2012
Accepted 13 July 2012

Keywords:
Angiography
Coronary
3D reconstruction
Stenosis
TIMI

ABSTRACT

Three dimensional coronary modeling and reconstruction can assist in the quantitative analysis of coronary flow velocity from 2-d coronary images. In this paper a novel method to assess coronary flow velocity is proposed. First, 3-d models of the coronary arteries are estimated from bi-plane X-ray images using epipolar constraint energy minimization for the selected fiducial points like bifurcations, and subsequently 3-d B-spline energy minimization for the arterial segments. A 4-d model is assembled from a set of 3-d models representing different phases of the cardiac cycle. The 4-d model is fitted to the 2-d image sequences containing basal or hyperemic blood flow information. Then, by counting the frames in analogy with TIMI frame counting, an index of the mean coronary flow velocity can be estimated. Our experimental results show that the algorithm correlates with $r = 0.98$ ($P<0.0001$, 95% CI 0.92–0.99) to the clinical measurements of the TFC.

1. Introduction

Coronary artery disease, or more specific a stenosis, may lead to a reduction in coronary blood flow. This is manifested in a reduced flow velocity of blood through the coronary arteries. TIMI frame counting [10] is a practical method to index blood flow velocity and quantize coronary flow velocity reserve using measurements in basal and hyperemic conditions. Coronary flow velocity reserve is an important measure for heart assessment [19,20,7]. In clinical practice the method of TIMI frame counting can be considered as a qualitative flow velocity assessment using 2-d monoplane X-ray images [22]. This method, however, is manually performed by a cardiologist and requires catheter measurements to provide information about vessel length. The standard minimally invasive modality to assess coronary arteries is mono-plane X-ray angiography, which is a two dimensional method. Three dimensional and also non-invasive methods are computed tomography (CT) and magnetic resonance imaging (MRI). Several 3-d semi-automatic modeling methods have been proposed using mono-plane [9] and bi-plane X-ray [6]. 4-d models with motion analysis are shown by Chen et al. [5] and [2]. Tomographic reconstruction techniques require multiple projection angles which are obtained in CT or rotational angiography. This requires measuring of the electrocardiogram to perform ECG-gated recording or retrospective ECG gated reconstruction. Tomographic reconstruction requires a calibrated system in which the projection geometry is well defined and at least three projections are required to get reasonable results [11]. Several improvements of this algorithm are proposed by [18,17,12]. Coronary models can be used, for example, in intervention planning [23] or fusion with other modalities like IVUS [15].

In this paper we propose a method using two standard, uncalibrated, mono-plane X-ray image sequences to create a 3-d model of the coronary arteries. Our main research goal is to automate the measurement of mean coronary flow velocity. In our previous research [3], we have aimed at using the 2-d X-ray angiography data directly, but quantization of flow velocity requires the length of the vessel which can only be obtained using 3-d information. Furthermore our 2-d analysis required coronary model fitting in which the model ideally should be 3-d. A set of 3-d models is created resulting in a 4-d model of the coronary arteries covering the complete cardiac cycle. This is accomplished by creating a temporal 3-d model using the basic 2-d X-ray information acquired by standard assessment procedures. A minimum of two projection angles is required to estimate a 3-d model from the 2-d data, as shown in Fig. 1.

The estimated 4-d model $\mathcal{T}$ is used as a template to find the coronary arteries in the 2-d X-ray images $\mathcal{I}$. A 3-d model is selected from $\mathcal{T}$ corresponding to the normalized cardiac phase of the 2-d image. Then, a 2-d projection of the 3-d model $\mathcal{M}$ is fitted onto the 2-d image by slightly adapting the 3-d model. This adaptation is controlled by deforming the 3-d model until the mean squared

* Corresponding author. Tel.: +31 53 489 2780; fax: +31 53 489 1060.
E-mail address: g.a.tenbrinke@alumnus.utwente.nl (G.A. ten Brinke).
[1] Tel.: +31 53 489 2780; fax: +31 53 489 1060.
[2] Tel.: +31 53 487 2110.

0895-6111/$ – see front matter © 2012 Elsevier Ltd. All rights reserved.
http://dx.doi.org/10.1016/j.compmedimag.2012.07.001

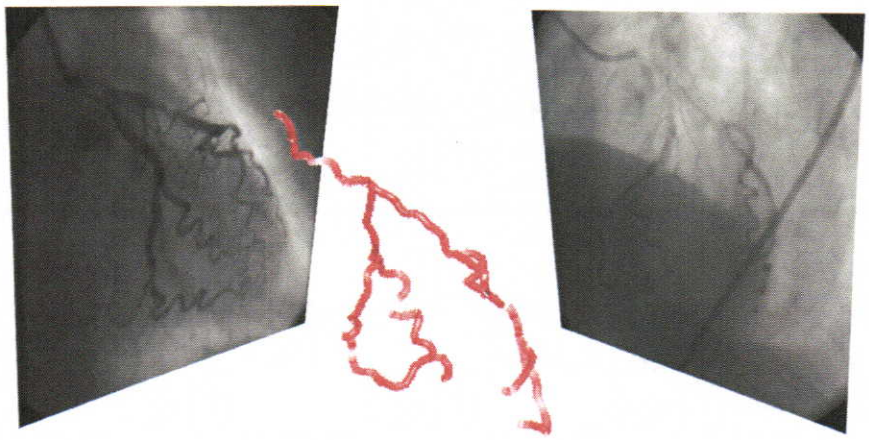

Fig. 1. 4-d model $\mathcal{T}$creation using mono-plane X-ray sequences at two different projection angles. The frames are selected using retrospective ECG gating. The 4-d cardiac cycle is covered by a set of 3-d models $\mathcal{T} = [\mathcal{M}_0, \ldots, \mathcal{M}_1]$ estimated from the 2-d images $\mathcal{I}$.

distance between the projection of the model wire-frame and the vessel centerlines in the 2-d image is minimized. This process is repeated for every image in the sequence.

After a satisfactory fit of the 3-d model the contrast agent density at the location of the vessel centerline is measured. Combining the 4-d model with these measurements results in a 4-d model including information about coronary blood flow from which we can estimate coronary blood flow velocity.

2. Methods

TIMI frame counting (TFC) is a manual method to give a flow velocity index by counting the number of frames between the appearance of the contrast agent at the main trunk and at the apical bifuraction of a vessel [10]. When the blood flow velocity is artificially increased by inducing hyperemic conditions using an injection of dipyradimole, papaverine or adenosine, the frame count is in general significantly decreased. The ratio between basal and hyperemic state frame counting can be defined as the frame count reserve. Flow limiting factors, such as the presence of a stenosis, will show a limited decrease of flow velocity during the hyperemic condition compared to basal conditions. Our approach to find TFC values automatically is to extract time density curves from the all images. These time density curves are represented as an image, called a contrast flow map, which is subsequently analyzed by standard image processing algorithms. In this paper we want to locate the vessels and measure, using densitometry, the contrast density at the vessel centerlines. Coronary vasculature is difficult to obtain from the low contrast images from only one 2-d view. It limits the temporal analysis of a single 2-d X-ray image sequence, because the information is not sufficient to resolve the ambiguities like vessel overlap and foreshortening. Therefore, we will reconstruct a 3-d model of the coronary arteries.

Fig. 2 clarifies the procedure. On top are the angiographic sequences used as input to the algorithm, we firstly use two sequences, the primary and secondary angular view, to estimate a 3-d coronary model. From the primary and secondary input sequence one cardiac cycle is selected which contains maximum opacifaction of the coronary arteries. In these images the start and end points of the main arteries and the most important bifurcations are manually annotated in one image resulting in a set of points. Then this annotation is propagated through the remaining images using template matching, the user is able to correct the automatic annotation. The annotated sequence covering one cardiac cycle from two viewpoints is used to create a 3-d model. This model is used to find the location of the vessels in the X-ray sequences of the basal and hypereamic acquisitions. The next section will explain this process in more detail.

2.1. Imaging geometry

The 3-d coronarary reconstruction method using planar X-ray images follows the computer vision methods described by Hartley and Zisserman [13]. After the creation of the model, the model is fitted to the two dimensional image sequence using 3-d deformation and projection. Finally, a densitometric measurement results in flow maps from which we can estimate TFC.

The center of the heart coincides with the center of rotation of the C-arm, this is because the images in this research are acquired with a full-view of the coronary arteries centered in the image-plane. A small center offset can sufficiently be corrected by a table motion correction algorithm, which is discussed in Section 2.4. From this point of view, we can use the uncalibrated information in the DICOM file to construct the geometry of the C-arm. In our case the known variables are the size of the image plane N in [pixels] and the width of the intensifier D in [mm]. We assume that the focal distance f in [mm] is equal to the distance source to detector. Based on this assumption we can calculate the detector element (pixel) size $\mu = D/N$. We also introduce a displacement vector in the image plane $\mathbf{d} = [d_x, d_y]$. Variables f, N and D can be extracted from the DICOM info structure from fields *Distance Source to Detector*, *Rows* and *Intensifier Size*, respectively. These variables define the camera calibration matrix K:

$$\mathbf{K} = \begin{bmatrix} f\mu & 0 & \frac{1}{2}N + d_x \\ 0 & f\mu & \frac{1}{2}N + d_y \\ 0 & 0 & 1 \end{bmatrix} \tag{1}$$

The rotation matrix R can be formed using the primary (RAO/LAO) and secondary angle (CAUD/CRAN) information from the DICOM info structure:

$$\mathbf{R}_x(\beta) = \begin{bmatrix} 1 & 0 & 0 \\ 0 & \cos(\beta) & -\sin(\beta) \\ 0 & \sin(\beta) & \cos(\beta) \end{bmatrix} \tag{2}$$

$$\mathbf{R}_y(\alpha) = \begin{bmatrix} \cos(\alpha) & 0 & \sin(\alpha) \\ 0 & 1 & 0 \\ -\sin(\alpha) & 0 & \cos(\alpha) \end{bmatrix} \tag{3}$$

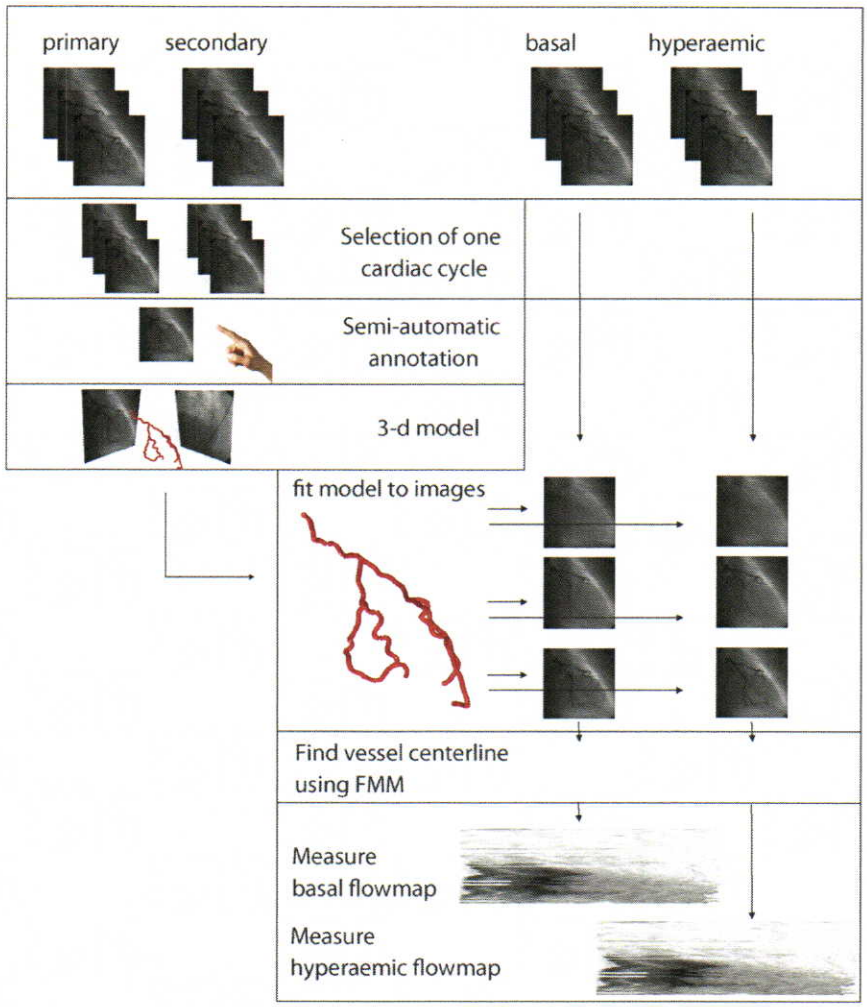

Fig. 2. Overview of the creation of flow maps from X-ray angiography image sequences.

$$\mathbf{R}(\alpha, \beta) = \mathbf{R}_x(\beta)\mathbf{R}_y(\alpha) \tag{4}$$

The primary angle corresponds to RAO ($\alpha \leq 0$) and LAO ($\alpha > 0$) projection and the secondary angle to the CAUD ($\beta \leq 0$) and CRAN ($\beta > 0$) projection, see Fig. 3. The translation vector $\mathbf{t}$ is the position of the camera relative to the center of rotation. The z-axis points towards the ceiling, so the camera is $f/2$ out of the center of rotation in z direction:

$$\mathbf{t} = \begin{bmatrix} 0 \\ 0 \\ f/2 \end{bmatrix} \tag{5}$$

The camera matrix is now:

$$\mathbf{P} = \mathbf{K}\left[\mathbf{Rt}\right] \tag{6}$$

2.2. 3-d modeling

Fallavollita and Cheriet [9] have proposed a method to estimate coronary arteries using snakes. Our method uses this approach with the main difference that a FMM speed-map is used as force function. The force function is important because it controls the deformation of the 3-d snake. The snake is described by a 3-d-curve or B-spline $v(s)$. The deformation is controlled by an energy minimization function:

$$E(v) = \int_0^1 (E_{int}(v) + E_{ext}(v))\, ds \tag{7}$$

where $E_{int}(v)$ is the internal energy, preserving smoothness, and $E_{ext}(v)$ is the external energy, attracting the snake to image features. E_{int} can be described by:

$$E_{int}(v) = \gamma \left| \frac{\partial v}{\partial s} \right|^2 + \lambda \left| \frac{\partial^2 v}{\partial s^2} \right|^2 \tag{8}$$

where γ and λ are constants controlling the tension and rigidity of the snake respectively.

The external energy E_{ext} can be described by:

$$E_{ext}(v) = \phi^{-1}(\mathbf{x}_1, \mathbf{x}_2, \mathbf{P}_1, \mathbf{P}_2) - \mathbf{X} \tag{9}$$

where ϕ^{-1} is the retro-projection operator. This operator reconstructs a 3-d point from two given 2-d points $\mathbf{x}_n$ in two projection planes $n = 1, 2$ described by camera matrix $\mathbf{P}_n$:

$$\mathbf{X} = \phi^{-1}(\mathbf{x}_1, \mathbf{x}_2, \mathbf{P}_1, \mathbf{P}_2) \tag{10}$$

$\mathbf{x}_n$ are the original points $\mathbf{q}_n$ with a movement depending on the force maps $\mathbf{F}_n$:

$$\mathbf{x}_n = \mathbf{q}_n - \nabla \mathbf{F}_n(\mathbf{q}_n) \tag{11}$$

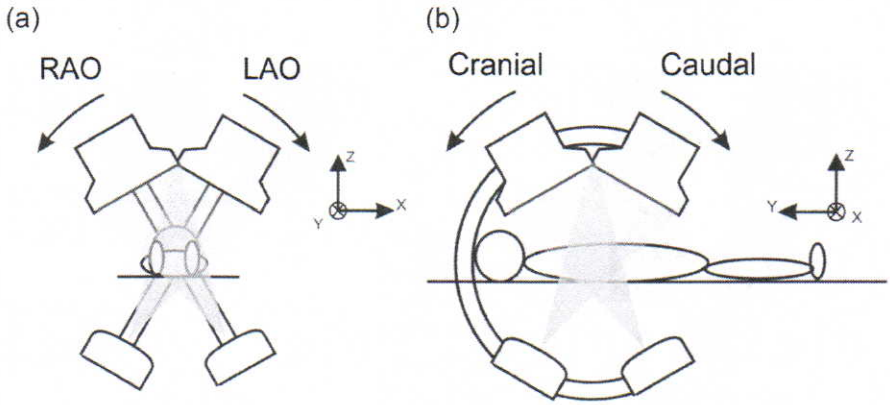

Fig. 3. The C-arm can rotate about two angles, the primary angle α (RAO/LAO), see Fig. 3(a), and the secondary angle β (Caudal/Cranial), see Fig. 3(b). The origin of the coordinate system is placed at the center of rotation of the C-arm. The C-arm is at anterior-posterior (PA) position when $[\alpha, \beta] = [0, 0]$. (a) Primary angle (α) and (b) secondary angle (β).

where $\mathbf{q}_n$ are the projections of v on projection planes $n = 1, 2$ and $\mathbf{F}_n$ are the used force maps, which will be discussed in the next section.

The numerical implementation of the snake algorithm requires approximation of the derivatives with finite differences. Conversion to vector notation with $v_i = (x_i, y_i, z_i)$ [1] results in:

$$E_{int}(v) = \gamma \left| v_i - v_{i-1} \right|^2 + \lambda \left| v_{i-1} - 2v_i + v_{i+1} \right|^2 \tag{12}$$

$$\begin{aligned} \gamma \left| \frac{\partial v_i}{\partial s} \right|^2 &\approx \gamma \left| v_i - v_{i-1} \right|^2 \\ &= \gamma \left((x_i - x_{i-1})^2 \right. \\ &+ (y_i - y_{i-1})^2 \\ &+ \left. (z_i - z_{i-1})^2 \right) \end{aligned} \tag{13}$$

$$\begin{aligned} \lambda \left| \frac{\partial^2 v_i}{\partial s^2} \right|^2 &\approx \lambda \left| v_{i-1} - 2v_i + v_{i+1} \right|^2 \\ &= \lambda \left((x_{i-1} - 2x_i + x_{i+1})^2 \right. \\ &+ (y_{i-1} - 2y_i + y_{i+1})^2 \\ &+ \left. (z_{i-1} - 2z_i + z_{i+1})^2 \right) \end{aligned} \tag{14}$$

The distance between the points is kept equidistant (Euclidean distance) by redistribution of the points along the snake using cubib B-spline interpolation. Discretization of the integral in Eq. (7) gives:

$$E = \sum_{i=0}^{N-1} (E_{int}(v_i) + E_{ext}(v_i)) \tag{15}$$

for a snake with N nodes.

Minimization of E allows us to rewrite Eq. (15) to be solved using dynamic programming:

$$\begin{aligned} E(v_1, v_2, \ldots, v_N) &= E_1(v_1, v_2) \\ &+ E_2(v_2, v_3) + \ldots \\ &+ E_{N-1}(v_{N-1}, v_N) \end{aligned} \tag{16}$$

In case of, for example, $N = 5$ nodes we can calculate the minimal energy using sub-functions $s_k(v_{k+1})$:

$$\begin{aligned} s_1(v_2) &= \min_{v_1} E_1(v_1, v_2) \\ s_2(v_3) &= \min_{v_2} (s_1(v_2) + E_2(v_2, v_3)) \\ s_3(v_4) &= \min_{v_3} (s_2(v_3) + E_3(v_3, v_4)) \\ \min_{v_1, \ldots, v_5} E(v_1, \ldots, v_5) &= \min_{v_4} (s_3(v_4) + E_4(v_4, v_5)) \end{aligned} \tag{17}$$

The recurrence relation is now stated as (for clarity the second order term is not presented):

$$s_k(v_{k+1}) = \min_{v_k} \left\{ s_{k-1}(v_k) + E_{ext}(v_k) + \left| v_{k+1} - v_k \right|^2 \right\} \tag{18}$$

Each stage consists of 26 possibilities, the neighbors $[3 \times 3 \times 3] - 1$, to calculate. The internal energy is stored at each stage. The indices of node position with the minimum energy cost are stored in the position matrix. The minimum energy can now be found by back-tracing in the position matrix using Dijkstra's shortest path algoritm [8].

2.3. Force map

The force map is specifically constructed for each vessel segment to prevent interference from other vessel segments during the minimization process of the 3-d-snake. The begin and endpoint of each vessel segment is annotated. With this annotation we can generate a force map from each vessel segment using the fast marching method (FMM) [21]. This force map is used to find the vessel centerline using the minimal cost path algorithm. The 2-d vesselcenterline is plotted in a 2-d grid. From this grid a euclidean distance map is calculated. The gradient of the distance map is used as force map in the snake energy minimization algorithm.

The vessel centerline is found using the 2-d multi-stencils fast marching method (FMM) [14]. This FMM is used to build a map containing the travel time between the start-point and all other points using a force function, which can be considered as the speed. The FMM solves the Eikonal equation:

$$\left\| \nabla T(x, y) \right\| F(x, y) = 1 \tag{19}$$

in which $T(x, y)$ is the arrival time of the front and $F(x, y)$ is the force function. The contrast enhanced image $I_c(x, y)$ is used as input $F(x, y)$ for the fast marching method:

$$F(x, y) = (1 - (G_\sigma \otimes I_c))^\gamma \tag{20}$$

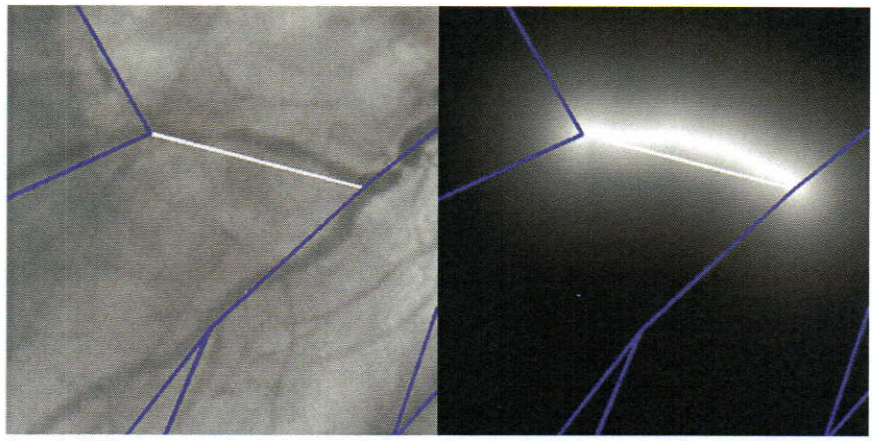

Fig. 4. The right image shows the annotation of the vessel segments with a highlight (in white) of the vessel segment currently being traced. The right image shows the euclidean distance map after vessel detection using the FMM method and minimal cost path algorithm. The gradient of the distance map is used as force field in the snake deformation algorithm.

Now the vessel centerline is the minimum cost path from the starting point to the end point, the back-tracing of the minimal cost past is performed using a fourth order Runge–Kutta approximation. The centerline, see Fig. 4, is defined by $v(s) = (x(s), y(s))$ where x and y are the coordinate functions and $s \in [0, 1]$ is the parametric domain which describes the vessel from start to endpoint.

2.4. Table motion compensation

Table motion is compensated using image plane shifting. The only requirement for this algorithm is the annotation of the catheter-tip throughout the image sequence. The correction is performed in the x–y plane of the local coordinate system, this results in a converging solution. Eq. (6) is changed to include the table translation in the x–y plane:

$$\mathbf{P} = \mathbf{K}\left[\mathbf{R}\left[\mathbf{t} + \mathbf{R}^{-1}\mathbf{t}_t\right]\right]; \tag{21}$$

in which $\mathbf{t}_t$ is the vector:

$$\mathbf{t}_t = \begin{bmatrix} x_t \\ y_t \\ 0 \end{bmatrix} \tag{22}$$

This vector has two parameters x_t and y_t. These parameters represent table motion, which results in an x–y motion in the image plane. The parameters can be solved by minimizing the re-projection error of the catheter-tip in the second image plane using Eq. (9). The method solves the triangulation problem using the direct linear transform. This method is described in detail in Hartley and Zisserman [13].

2.5. Fitting

The 3-d model is fitted to each frame in the image sequence from which we want to measure the TFC. The vessel centerline is obtained using the FMM method. The start and end points of the vessel segment are determined by projection of the segments of the 3-d model. Most likely, the projection of the segment will not fit the vessel centerline found by the FMM method. Therefore, the 3-d model is iteratively deformed until the vessel centerline coincides with the projection of the segment. We allow a maximum of 10 iterations of the model deformation to prevent over-fitting when a vessel centerline is incorrectly found due to low or none contrast density.

2.6. Annotation

Three dimensional reconstruction from a limited set of projections (N_p=2) is a challenging task. Therefore we have created a ground truth dataset using semi automatic annotation of our dataset. The process of annotating the dataset is based on our flow estimation software as described in ten Brinke et al. [3]. We have discarded image pre-filtering with coherence filters and vessel segmentation algorithms to prevent error accumulation and experimental thresholds.

The user selects an image from the dataset with maximum opacified arteries. Next, the vessel structure is annotated by selecting bifurcations and endpoints. These points are denoted $\mathcal{P}_i(x, y)$. Points are interconnected using segments which are stored in a connection matrix $\mathcal{C}_{i,j}$ connecting point $\mathcal{P}_i$ with point $\mathcal{P}_j$. It is a redundant matrix, so only the upper triangle is used. All points can be labeled $\mathcal{L}_i$, for example 'LAD', 'LCx', 'Cathetertip'. A dataset contains the annotation set $\mathcal{S} = \{\mathcal{P}(n), \mathcal{C}, \mathcal{L}\}$ in which $n = [1 \ldots N]$, with N the number of images in the dataset. So each image shares the same labels, interconnections and amount of points, only the locations of the points vary. This allows the creation of a temporal 3-d model using accurate data points. The user can use fast marching assistance for tracing the vessel centerline to make sure that the annotation correctly follows the vessels. All other frames are semi-automatically annotated using template matching.

2.7. Contrast flow map analysis

From the DICOM file we obtain 8-bit grayscale images with a size of [512 × 512] pixels. The raw data will be used to construct the contrast flow map, which results in a flow map with the same resolution as the images. Each line in the flow map represtent the contrast agent density along one vessel centerline $s = [0 \ldots 1]$, with in the vertical direction the image index $n = [1..N]$, see Fig. 5. In this research we will focus on the most clearly visible vessel, which is the LAD. The contrast flow map is analyzed using the following image processing steps: The mean value is removed from the single frame measurements. This mean value Γ_{mean} is the mean from all single measurements in the temporal direction:

$$\Gamma_{mean}(n, s) = \Gamma(n, s) - \frac{1}{N}\sum_{n=0}^{N-1}\Gamma(n, s) \tag{23}$$

for $s = [0..1]$. Next we calculate a threshold using a 256 bins histogram from Γ_{mean}. In general, the maximum peak in the histogram

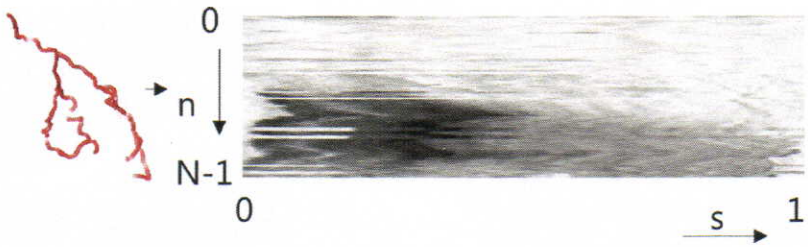

Fig. 5. Densitometry is applied on each image. The result is the measurement of the contrast density at the location of the vessels. This information is shown in a flow-map for each vessel. From this the coronary flow velocity can be estimated.

belongs to the contrast agent (dark) values. In practice, we can separate the opacified arteries from the transparent arteries using a threshold consisting of the maximum peak position in the histogram plus the standard deviation of the peak which is empirically set at 1/8 of the total number of bins.

This threshold is then applied to the contrast flow map. A Canny [4] edge detector finds the lines in the contrast flow map. One line (or curve) in the contrast flow map connects the arrival times and vessel positions of the contrast agent. The assumption that the contrast agent propagates with a constant velocity through the arteries allows us to use a line fit. The lines are detected using the Hough transform [16]. The slope of the line is related to the contrast flow velocity. All lines that do not have a negative slope are discarded as well as lines with a starting point after 1/2 of the total acquisition time (we assume that the coronary arteries will be fully opacified by the injection of the contrast agent in the first half of the recorded image sequence).

3. Experiments

Two experiments are conducted: using a static brass model, see Fig. 6, imaged using a Phillips Xper X-ray scanner and with clinical data.

Our clinical dataset contains images of interventions with specific TIMI frame counting data and coronary artery length measurements. The coronary artery length is clinically measured using a catheter starting from the left main artery to the apical bifurcation of the LAD. It contains 32 patients (11 female, 21 male) from which two assessments are discarded because they do not contain at least two different projection angles of the left-coronary artery. From the resulting 30 patients a total of 13,096 images have been semi-automatically annotated. The two visually best series are selected for annotation taking into account a large angular distance between the series, allowing to recreate a 3-d model. Note that, in constrast to the catheter measurements, in the measurements of the reconstructed coronary arteries we only measure from the start of the LAD to the apical bifurcation.

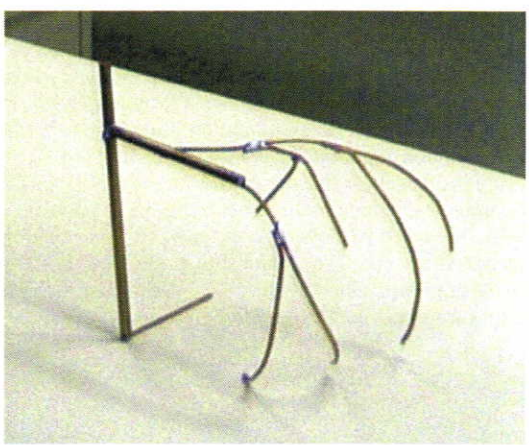

Fig. 6. The brass coronary phantom

4. Results

4.1. Phantom

We have tested the 3-d modeling algorithm on the brass phantom. A fully automatic reconstruction of the vessel segments based on epipolar line matching was not successful due to the unknown camera calibration parameters. In the literature methods are proposed by e.g. Blondel et al.[2] to address this problem. Since it is not the focus of our research to create reconstruction algorithms we have decided to manually annotate the vessel segments. With the manual annotation and the B-spline algorithm proposed by Fallavollita and Cheriet [9] we were able to create usable models from the 2-d data. Fig. 7 shows the reconstruction of the phantom and Table 1 shows the errors made in the reconstruction. Large variations are visible at the vesselsegements which are not clearly visible in both images.

4.2. Clinical data

The quality of the coronary models is characterized by the reprojection error. The length of the LAD is known from catheter measurements, so we will compare the LAD length measured from the model with the ground truth of the catheter measurement. The results are displayed in Fig. 9.

Overall results are depicted in Fig. 10(a). The measured TFC correlates with the clinical measurements with $r = 0.80$ ($P<0.0001$, 95% CI 0.63–0.89).

From 14 of 32 patients we have data of completely opacified coronary arteries during one cardiac cycle from two viewing angles. This data is used to create models covering the complete cardiac cycle. In Fig. 8 an example of 3-d models created from 5 phases of

Table 1
Reconstruction results of the phantom. See Fig. 7 for the segment locations.

Segment	μ_1 [pixels]	σ_1 [pixels]	μ_2 [pixels]	σ_2 [pixels]
1	8	± 8	78	± 37
2	10	± 8	5	± 3
3	39	± 32	4	± 2
4	64	± 48	6	± 6
5	8	± 8	2	± 1
6	35	± 31	14	± 7
7	3	± 2	87	± 58
8	6	± 5	57	± 33
9	2	± 1	1	± 1
10	2	± 0	2	± 1
11	2	± 1	3	± 2
12	3	± 1	3	± 2
13	7	± 6	3	± 1

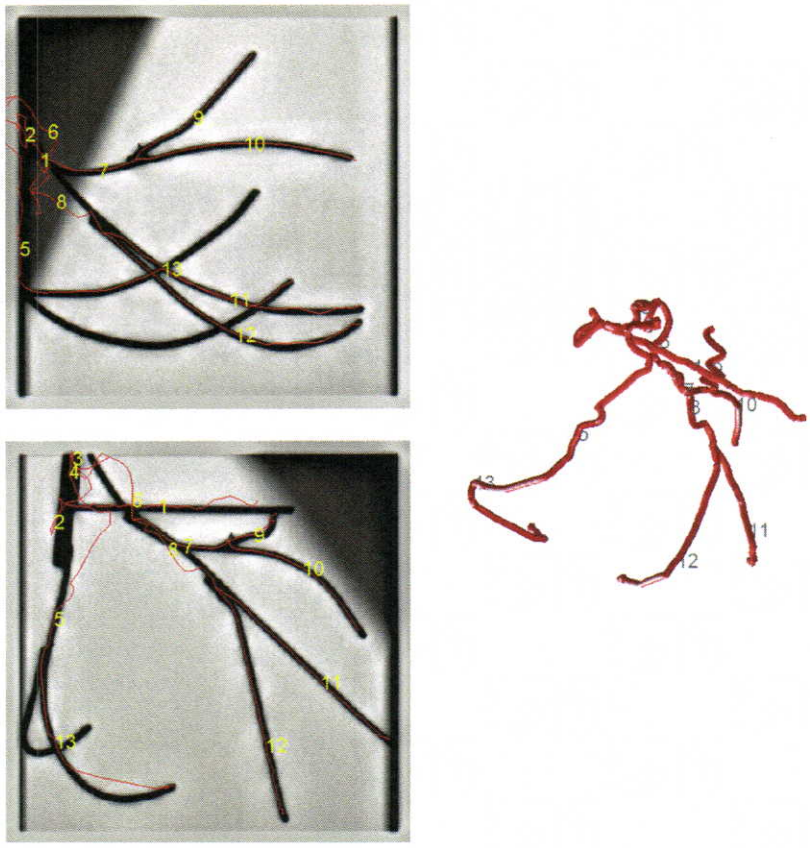

Fig. 7. Reconstruction of phantom. See Table 1 for the reconstruction results.

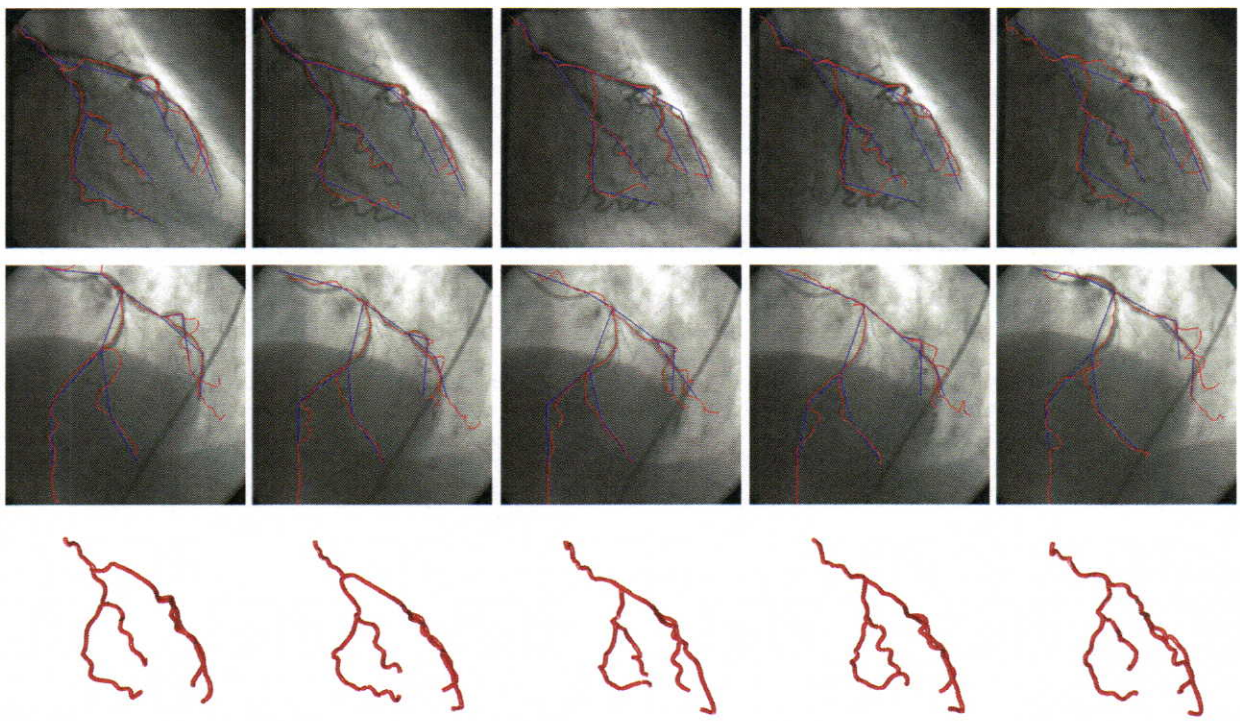

Fig. 8. Modeling of the coronary arteries. The first and second row show the two images used in the modeling, the third row shows the generated model. A total of 20 models are created to cover the complete cardiac cycle, only 5 are shown in this figure. (For interpretation of references to color in the text, the reader is referred to the web version of this article.)

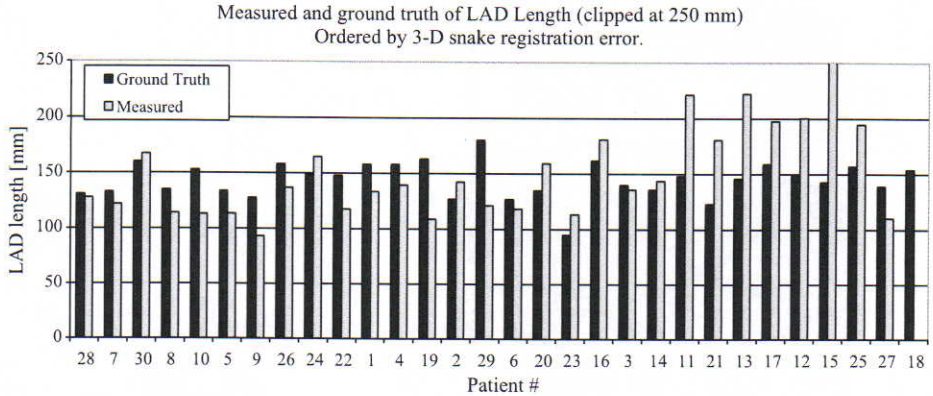

Fig. 9. Length of the left anterior descending (LAD) artery. The length calculated from the 3-d model is compared to the length measured with a catheter (ground truth). The patients are ordered by registration error. The registration error is a measure for the accuracy of the LAD length measurement.

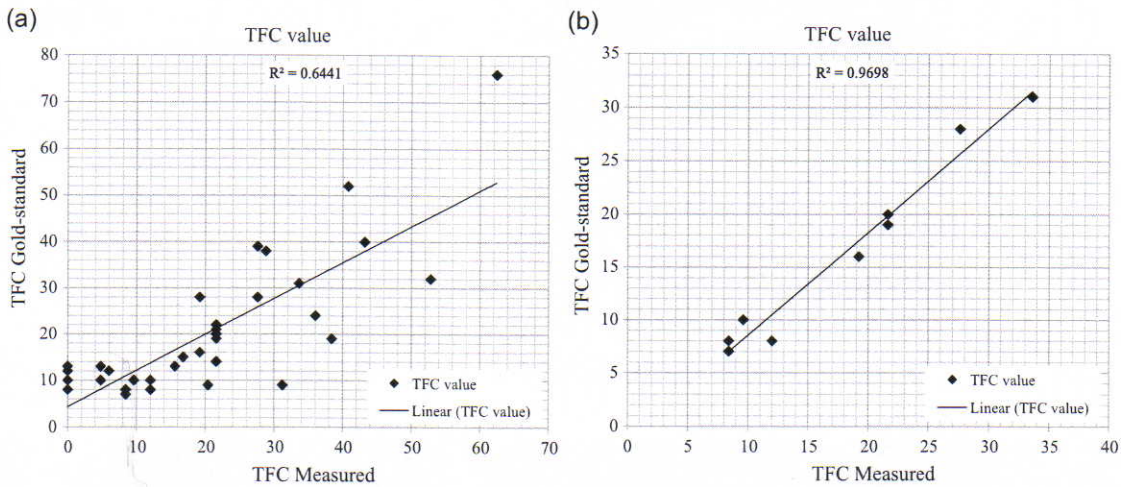

Fig. 10. Scatter-plots showing the correlation between the measured (using 3-d modeling and flow measurements) and the ground thruth (measurements performed by a cardiologist). (a) Scatter-plot with linear fit of the measured and ground truth TFC values of the 32 patients. (b) Scatter-plot with linear fit of the measured and ground truth TFC values of the remaining 9 patients.

the cardiac cycle are shown. Retrospective gatng is used to select two images for the creation of one 3-d model, the figure shows semi-automatically annotation of the vessels in blue and the 2-d projection of the final model in red. The 2-d projection of the model does not exactly fit the X-ray image, but that is not a main issue because the 3-d model is deformed to fit the X-ray image in a latter phase. From 9 of these 14 patients we were able to obtain a measured TFC within the intra-observer variability range of ±5 frames. The measured TFC correlates with the clinical measurements with $r = 0.98$ ($P<0.0001$, 95% CI 0.92–0.99). See Fig. 10(b).

5. Discussion

The accuracy of the algorithm depends on clinical and technological limitations. Acquisition of high quality images is limited by the amount of X-ray exposure to the patient and the clinician. Therefore, the clinician tries to minimize the X-ray dose by highly effective usage of the field of view. This results in table motion during the acquisition and a minimum amount of images. Also, toxic effects of contrast agent limit the amount of image aquisition runs. Dose limitation results in lower quality images or incomplete opacification of the coronary structure. Furthermore, the health condition of the patient may limit the usage of the breath hold technique. Moreover, patient arrhythmias during acquisitions may occur spontaneous or due to the injection of contrast agents or vasodilators. Finally, patient dimensions influences the amount of X-ray required and as a result changes the brightness of the images. This may vary at different acquisition angles.

The clinical acquisition problems immediately have an effect on the performance of the analysis software: for 3-d modeling, a calibrated X-ray system is required. System calibration allows epipolar matching and quantized models. Also, the creation of a temporal model requires one completely opacified coronary vessel structure during the whole cardiac cycle. For 3-d modeling it also requires to have this from a minimum of two different angles. Ambiguity still exists, but can be reduced using the B-spline models of the vessel segments. Patient motion like breathing and table motion result in motion artifacts. The results of these motions are inaccurate models. We have minimized these errors by annotating the catheter-tip and applying motion correction by aligning the catheter-tips in both imaging planes.

During an X-ray acquisition, several image enhancements may affect the analysis software. Automatic exposure control, for example, results in an extra variable which should be included in densitometric measurements. This variable, however, is not updated during the acquisition. Anatomical background structures, like the spinal cord, influence vessel tracing algorithms. Theoretically we can use a background subtraction algorithm, in practice,

motion artifacts prevent its application. In this research 3-d modeling is used to compensate for that.

5.1. Limitations

The method discussed in this paper can only be used when at least two acquisitions are available with a complete opacification of the coronary arteries during one complete cardiac cycle. The time resolution of the measurements is limited by the frame-rate of the X-ray equipment. In normal acquisitions this frame-rate is 12.5 or 15 frames per second (fps), resulting in respectively 80 ms or 66.7 ms maximum temporal resolution (without interpolation) depending on the acquisition device. Acquisitions with 50 fps are technically no problem, however, clinically not desired because of higher X-ray exposure to patient and clinician.

5.2. Conclusion

In this paper we have proposed a method towards the automation of TIMI frame counting and, as a result of that, the measurement of coronary flow velocity reserve using standard angiographic X-ray acquisition. It requires a full cardiac cycle of completely opacified coronary arteries from at least two different angular positions recorded with ECG and an additional run for the hyperemic measurement. From 9 patients we were able to obtain a measured TFC within the intra-observer variability range of ±5 frames. The measured TFC correlates with the clinical measurements with $r = 0.98$ ($P<0.0001$, 95% CI 0.92–0.99).

Acknowledgments

The authors thank M. Eskes B.Sc. and P. Gooskens B.Sc. for annotation of the dataset used in this research.

References

[1] Amini A, Weymouth TE, Jain RC. Using dynamic programming for solving variational problems in vision. IEEE Trans Pattern Anal Mach Intell 1990;12(9):855–67.
[2] Blondel C, Malandain G, Vaillant R, Ayache N. Reconstruction of coronary arteries from a single rotational X-ray projection sequence. IEEE Trans Med Imaging 2006;25(5):653–63.
[3] ten Brinke GA, Slump CH, Storm CJ. Digital densitometric determination of clinical relative coronary flow distributions. In: Proceedings of the SPIE, vol. 6143. International Society for Optical Engineering, 2006.
[4] Canny J. A computational approach to edge detection. IEEE Trans Pattern Anal Mach Intell 1986;8:679–98.
[5] Chen SYJ, Carroll JD. Kinematic and deformation analysis of 4-D coronary arterial trees reconstructed from cine angiograms. IEEE Trans Med Imaging 2003;22(6):710–21.
[6] Chen SYJ, Metz CE. Improved determination of biplane imaging geometry from two projection images and its application to three-dimensional reconstruction of coronary arterial trees. Med Phys 1997;24:633.
[7] Csizmadia NP, Schrijver M, Slump CH, Lubbers APG. Digital densitometric determination of relative coronary fllow distributions. Med Biol Eng Comput 2001;39:303–9.
[8] Dijkstra EW. A note on two problems in connexion with graphs. Numerische Mathematik 1959;1(1):269–71.
[9] Fallavollita P, Cheriet F. Optimal 3D reconstruction of coronary arteries for 3D clinical assessment. Comput Med Imaging Graph 2008;32(6):476–87.
[10] Gibson CM, Cannon CP, Daley WL, Dodge JT, Alexander B, Marble SJ, McCabe CH, Raymond L, Fortin T, Poole WK. TIMI frame count a quantitative method of assessing coronary artery flow. Circulation 1996;93(5):879–88.
[11] Gordon R, Bender R, Herman GT. Algebraic reconstruction techniques (ART) for three-dimensional electron microscopy and X-ray photography. J Theoret Biol 1970;29(3):471–81.
[12] Hansis E, Schäfer D, Dössel O, Grass M. Evaluation of iterative sparse object reconstruction from few projections for 3- rotational coronary angiography. IEEE Trans Med Imaging 2008;27(11):1548.
[13] Hartley R, Zisserman A. Multiple view geometry in computer vision. Cambridge University Press; 2000.
[14] Hassouna MS, Farag AA. Multistencils fast marching methods: A highly accurate solution to the eikonal equation on cartesian domains. IEEE Trans Pattern Anal Mach Intell 2007;29(9):1563–74.
[15] Hoffmann KR, Wahle A, Pellot-Barakat C, Sklansky J, Sonka M. Biplane X-ray angiograms intravascular ultrasound and 3D visualization of coronary vessels. Int J Cardiac Imaging 1999;15(6):495–512.
[16] Illingworth J, Kittler J. A survey of the hough transform. Comput Vision Graph Image Process 1988;44(1):87–116.
[17] Li M, Kudo H, Hu J, Johnson RH. Improved iterative algorithm for sparse object reconstruction and its performance evaluation with micro-CT data. IEEE Trans Nucl Sci 2004;51(3):659–66.
[18] Li M, Yang H, Kudo H. An accurate iterative reconstruction algorithm for sparse objects: application to 3D blood vessel reconstruction from a limited number of projections. Phys Med Biol 2002;47(15):2599–609.
[19] Reiber JHC, Serruys PW, Slager CJ. Quantitative coronary and left ventricular cineangiography: methodology and clinical applications. Developments in cardiovascular medicine. Boston, Dordrecht: Nijhoff; 1986.
[20] Schrijver M. Angiographic image analysis to assess the severity of coronary stenosis. Ph.D. thesis, University of Twente; 2002.
[21] Sethian JA. Evolution implementation and application of level set and fast marching methods for advancing fronts. J Comput Phys 2001;169(2):503–55.
[22] Stoel MG, Zijlstra F, Visser CA. Frame count reserve. Circulation 2003;107(24):3034–9.
[23] Wink O, Kemkers R, Chen SY, Carroll JD. Intra-procedural coronary intervention planning using hybrid 3-dimensional reconstruction techniques. Acad Radiol 2003;10(12):1433–41.